ACS Photonics

Letter

pubs.acs.org/journal/apchd5

Nonlinear Interference and Tailorable Third-Harmonic Generation from Dielectric Oligomers

Maxim R. Shcherbakov,*[,†] Alexander S. Shorokhov,[†] Dragomir N. Neshev,[‡] Ben Hopkins,[‡] Isabelle Staude,[‡] Elizaveta V. Melik-Gaykazyan,[†] Alexander A. Ezhov,[†] Andrey E. Miroshnichenko,[‡] Igal Brener,[§] Andrey A. Fedyanin,[†] and Yuri S. Kivshar[‡]

[†]Faculty of Physics, Lomonosov Moscow State University, Moscow 119991, Russia

[‡]Nonlinear Physics Centre, Research School of Physics and Engineering, The Australian National University, Canberra ACT 0200, Australia

[§]Center for Integrated Nanotechnologies, Sandia National Laboratories, Albuquerque, New Mexico 87185, United States

S *Supporting Information*

ABSTRACT: It is known that the nonlinear optical properties of photonic nanostructures can be modified substantially due to strong field confinement and optical resonances. In this contribution, we study third-harmonic generation from low-loss subwavelength silicon nanodisks arranged in the form of trimer oligomers with varying distance between the nanoparticles. Each of the nanodisks exhibits both electric and magnetic Mie-type resonances that are shown to affect significantly the nonlinear response. We observe the third-harmonic radiation intensity that is comparable to that of a bulk silicon slab and demonstrate a pronounced reshaping of the third-harmonic spectra due to interference of the nonlinearly generated waves augmented by an interplay between the electric and the magnetic dipolar resonances.

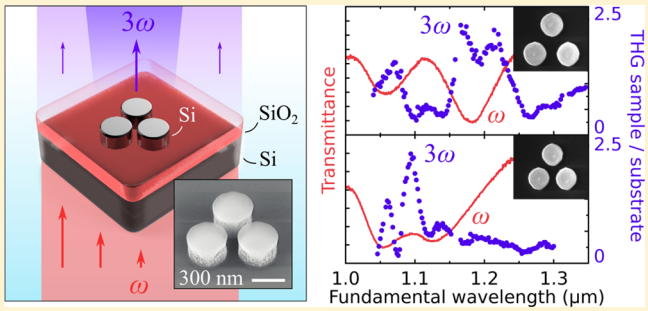

KEYWORDS: *nonlinear optics, third-harmonic generation, silicon nanoparticles, nanoparticle oligomers, optical magnetism, Mie scattering*

Nonlinear optical properties of photonic and plasmonic nanostructures are known to differ substantially from the properties of bulk materials due to strong subwavelength confinement and localized resonances.[1] In particular, a pronounced modification of the second-order nonlinear response has been observed in arrays of metallic subwavelength holes[2,3] and lattices of metallic chiral nanoparticles,[4] and it was demonstrated that the strong enhancement of the local fields with the formation of "hot spots" can improve the nonlinear optical processes efficiency in these nanostructures.[1] Similarly, third-harmonic generation (THG) was very recently observed in metallic nanoantennas,[5] complex plasmonic Fano nanostructures,[6] and plasmonic metacrystals,[7] where an enhancement of the THG signal was demonstrated in the presence of electric resonances. In contrast, the effect of magnetic resonances on the nonlinear properties of nanostructures is much less studied and, until recently, was limited to plasmonic structures such as split-ring resonators,[8,9] fishnet metasurfaces,[10,11] and L-shaped plasmonic nanoparticles.[12] However, the nonlinear frequency generation in plasmonic nanostructures suffers from strong losses of metals at optical frequencies, losses that are further enhanced near the resonances.

To overcome this problem, we recently studied third-harmonic generation from individual silicon nanodisks and their periodic arrangements, and we demonstrated that the field localization at the magnetic resonance can result in 2 orders of magnitude enhancement of the third-harmonic (TH) intensity with respect to unstructured bulk silicon.[13] These high-permittivity, dielectric nanoparticles are emerging as a promising alternative to metallic nanoparticles for a wide range of nanophotonics applications; such nanoparticles exhibit both electric and magnetic multipolar resonances in the visible and near-IR spectral range.[14,15] In combination with their very low losses, these nanoparticles and their composites offer many unique opportunities for tailoring their nonlinear optical response. Interestingly, when nonlinearities of both electric and magnetic origin are present, the nonlinear response can be both modified substantially and accompanied by nonlinear interference, magnetoelectric coupling, and wave mixing effects, which have, so far, only been studied for microwave metamaterials and a few limited geometries.[16,17]

In this Letter, we study experimentally optical nonlinear effects originating from the resonant magnetoelectric response of all-dielectric symmetric oligomers composed of three silicon nanoparticles. Silicon nanoparticle oligomers have previously

Received: February 13, 2015
Published: April 27, 2015

DOI: 10.1021/acsphotonics.5b00065
ACS Photonics 2015, 2, 578−582

been studied in the linear regime.[18] Since silicon is a material with high third-order susceptibility,[19] we observe strong nonlinear phenomena in the optical response of high-index nanoparticles, and analyze how the spectral shape of the generated harmonic field depends on the distance between the nanoparticles in the structure. We reveal that both electric and magnetic Mie-type resonances can substantially enhance the intensity of the third-harmonic radiation, and we observe an interplay of electric and magnetic resonances with a strong reshaping of the third-harmonic spectra via the Fano-like interference[20] of nonlinearly generated optical waves, interference which we term below as "nonlinear interference."

RESULTS AND DISCUSSION

The silicon nanodisk trimers were fabricated via electron-beam lithography on backside polished silicon-on-insulator wafers with the top silicon layer of 260 nm. A scanning electron micrograph of a typical trimer is shown in the inset of Figure 1.

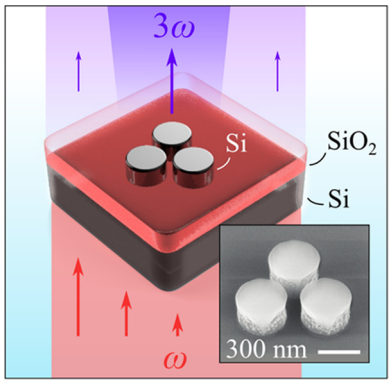

Figure 1. Illustration of the third-harmonic generation process in silicon nanodisk trimers. The IR pump beam illuminates the back of a silicon-on-insulator substrate with an array of nanodisk trimers fabricated out of the 260 nm thick top silicon layer. Exciting Mie-type electric and magnetic dipolar resonances with controlled spectral positions allows for a considerable enhancement of the THG by nanodisks as compared to the silicon substrate. Inset: oblique-view SEM image of a nanodisk trimer.

Different samples of trimers were fabricated, featuring an exposure-dose controlled variation of the diameter (d) of the individual nanodisks. The trimers were arranged in a square lattice with the lattice constant fixed to $p = 2$ μm. In addition, samples with different nominal center-to-center spacing (D) between the individual nanodisks within the trimer were fabricated. The nanodisks are known to demonstrate pronounced resonant electric and magnetic response in the near-IR,[21] and therefore, varying the nanodisk diameter, d, and the distance between nanodisks, D, allows for precise engineering of the mutual position of the electric and magnetic resonances of the trimers. The dimensions of the trimers are given in Table 1. The presence of the electric and magnetic dipolar resonances is verified by linear transmission spectroscopy as shown in Figure 2 with red curves for two sets of d and D: well-separated nanodisks with $d = 374$ nm and $D = 551$ nm, and close-packed nanodisks with $d = 349$ nm and $D = 365$ nm. Two pronounced minima could be observed in both of the transmittance spectra; the short-wavelength one being the Mie-type electric dipolar (ED) resonance and the long-wavelength one being the magnetic dipolar (MD) resonance. This can be established by comparing the spectra to those resulting from the multipole decomposition, as described in the Supporting Information.

Table 1. Main Parameters of the Samples: Nanodisk Diameter, Interparticle Distance within the Trimers, And Electric and Magnetic Resonance Position Values[a]

sample number	nanodisk diameter, d (nm)	center-to-center distance, D (nm)	electric resonance position (μm)	magnetic resonance position (μm)
1	349	465	1.053	1.126
2	347	553	1.054	1.143
3	367	460	1.054	1.165
4	371	461	1.059	1.168
5	367	552	1.057	1.171
6	371	556	1.057	1.175
7	374	551	1.058	1.181

[a]The geometrical parameters are designed in a way that the electric resonance retains its position within a 5 nm corridor, while the magnetic one has different position values. The listed quantities are extracted from SEM images. The statistical errors are 2 nm for d, 5 nm for D, and 3 nm for the resonance positions.

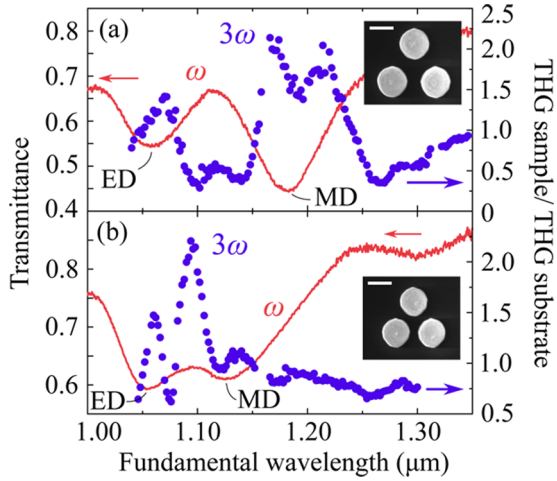

Figure 2. Tuning the TH spectral response (purple dots) of the silicon nanodisk trimers via the resonance properties of and the coupling strength between its constituent elements: (a) shows a trimer with well-separated nanodisks and (b) shows a trimer with close-packed nanodisks. Transmittance spectra (solid red curves) reveal the spectral position of the electric dipolar (ED) and magnetic dipolar (MD) resonances. The magnetic resonance position is tuned by varying both the distance between the nanodisks and their diameters. The THG spectrum normalized to the TH signal from the substrate away from the sample indicates a qualitatively different nonlinear response in the well-separated and close-packed trimer cases. The insets show the scanning electron micrographs of the trimers with the scale bar set at 300 nm.

Exciting the Mie-type resonances is expected to lead to an enhancement of the local electromagnetic fields inside the nanodisks. Since the third-order nonlinear polarization is proportional to the cube of the local electric field, enhanced local fields lead to a boost in the nonlinear optical conversion. We verify this by comparing the THG from the samples to the THG generated by the bulk silicon substrate underneath, both measured by our custom-built THG spectroscopy setup (see Methods and Supporting Information). Purple dots in Figure 2 show the THG spectra for the trimers with well-separated and close-packed nanodisks; notably, a mere 55 nm shift in the MD resonance wavelength results in strong qualitative changes in

DOI: 10.1021/acsphotonics.5b00065
ACS Photonics 2015, 2, 578−582

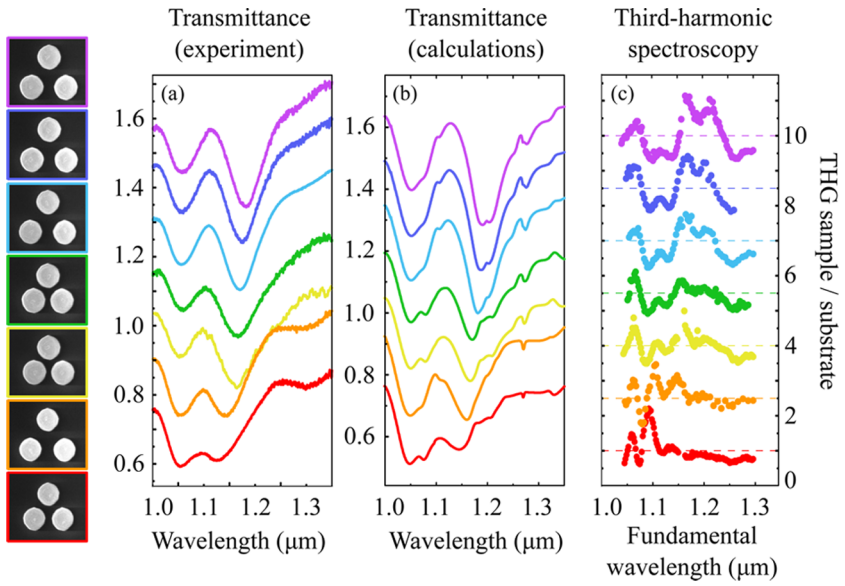

Figure 3. Controlling the TH response by adjusting the magnetic dipolar resonance position. (a) Experimental transmittance spectra for the nanodisk trimer samples revealing the gradual shift of the magnetic dipolar resonance peak of up to 55 nm. The spectra are vertically shifted by 0.15 units with respect to each other for better readability. (b) Corresponding numerical transmittance spectra of the trimer arrays. (c) Normalized THG spectra for the samples under study showing the evolution of the interference pattern as the resonances are brought closer to each other. A vertical displacement of 1.5 units is introduced between individual spectra for better readability. The dashed lines show the baseline denoting the condition $THG_{sam} = THG_{sub}$. The leftmost part of the figure shows SEM images of the corresponding trimers with color-coded outlines matching the colors of their respective spectra.

the THG spectrum. Specifically, if the resonances are separated spectrally, the enhancement effect is observed separately for the ED resonance at $\lambda = 1.058$ μm and for the MD resonance at $\lambda = 1.181$ μm. In contrast, bringing the ED and MD resonances together by closer arrangement of the nanodisks provides an extra resonant feature in the spectrum in between the resonances at $\lambda = 1.095$ μm. Moreover, this feature leads to a higher THG yield than that at the resonances themselves. This enhancement points out the importance of the interplay of the simultaneous excitation of ED and MD resonances. The smooth transition from individual to collective ED and MD regimes of the THG is shown in Figure 3c for a set of seven trimer arrays with the dimensions, as given in Table 1. Note that, due to the lower penetration depth of the TH radiation into Si and a lower density of disks, the observed enhancement factors are roughly 1.5 orders of magnitude below the results reported previously for a single-disk system.[13] In addition to the THG spectra, Figure 3 contains the corresponding linear transmittance spectra, which shows good agreement between the experiment and the spectra calculated numerically with CST Microwave Studio and shown in Figure 3b. The subtle oscillations and apparent peak splitting observed in the calculated spectra supposedly result from the periodic arrangement of the trimers and the plane-wave excitation used for our simulations. This is confirmed by the fact that the oscillations are absent in the experiment, where the incident beam had a finite numerical aperture, and, therefore, the diffractive coupling effect was smeared out. Note that, in accord with previous works,[22] we set the nanodisks to have 50 nm less diameter than measured with SEM from the top, due to an overetching of silicon as observed in the inset of Figure 1.

To get a deeper insight into the possible origin of the complex multipeak patterns observed in the THG spectra, we consider interference of the nonlinearly generated TH waves radiated by different parts of the sample, as illustrated schematically in Figure 4. Specifically, it is reasonable to consider two main sources of the THG: a nonresonant background contribution from the bulk silicon slab E_{back} and a

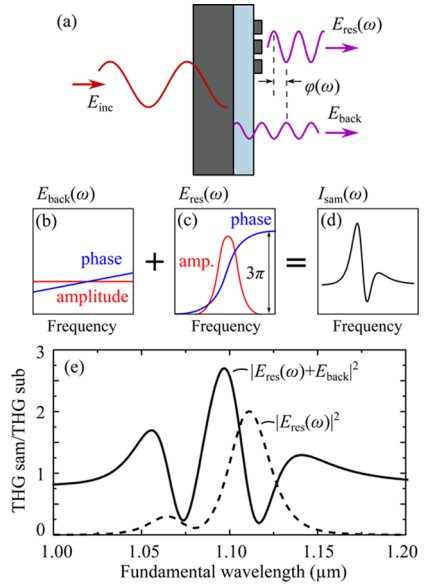

Figure 4. Explanation of the experimental THG patterns. (a) Schematic of the experiment. The observed THG signal consists of the resonant TH field $E_{res}(\omega)$ generated by the trimers and the background TH field E_{back} generated by the substrate. The sample can supply the background (b) and resonant (c) contributions to generate an asymmetric interference pattern (d) analogous to the Fano lineshape. (e) With two resonances present in the system, the experimental three-peak pattern observed in Figure 2b can be reproduced by plotting $|E_{res}(\omega) + E_{back}|^2$ given by eq 3. The dashed line gives the calculated TH signal that would have been detected in the absence of the substrate beneath the trimers.

DOI: 10.1021/acsphotonics.5b00065
ACS Photonics 2015, 2, 578−582

resonant contribution from the nanodisks $E_{res}(\omega)$. The spectra of the amplitude and phase of the respective contributions are shown in Figure 4b and c, respectively. The observed THG spectra are a consequence of the far-field interference of the above contributions, as illustrated in Figure 4d:

$$I_{sam}(\omega) \propto |E_{res}(\omega) + E_{back}|^2 \quad (1)$$

Under the conditions of similar contributions $E_{res} \approx E_{back}$ the spectrum is expected to exhibit pronounced oscillations, since E_{res} is highly dispersive with a remarkable 3π phase jump over the resonance (a phase jump in THG which corresponds to the standard π phase jump from a single, linear, Mie-type resonance). The contribution of the THG spectra from the disks $E_{res}(\omega)$ can then be written in terms of two components; one from the ED resonance and one from the MD resonance:

$$E_{res}(\omega) = \left(\frac{A\gamma}{\omega - \omega_E + i\gamma}\right)^3 + \left(\frac{B\gamma}{\omega - \omega_M + i\gamma}\right)^3 \quad (2)$$

where A and B are the amplitudes of the electric and magnetic resonance contributions, ω_E and ω_M are the central frequencies of the respective resonances, and γ is the (radiative) damping constant of the resonances, which is assumed to be the same for both resonances as deduced from the transmittance spectra in Figure 3a. We can then rewrite the expression for the observed THG signal in eq 1 as

$$I_{sam}(\omega) \propto \left|\left(\frac{A\gamma}{\omega - \omega_E + i\gamma}\right)^3 + \left(\frac{B\gamma}{\omega - \omega_M + i\gamma}\right)^3 + C\right|^2 \quad (3)$$

where C is a fitting coefficient that is responsible for the nonresonant reflection of the substrate THG by the nanodisk trimers. Equation 3 is plotted in Figure 4e (black curve) for the following fitting parameter values: $A = 0.9$, $B = 1.15$, $C = 0.9e^{-0.3i}$, $\gamma = 4 \times 10^{13}$ s^{-1}, $\omega_E = 1.76 \times 10^{15}$ s^{-1} ($\lambda = 1.07$ μm), $\omega_M = 1.70 \times 10^{15}$ s^{-1} ($\lambda = 1.11$ μm). Although these values were set as the fitting parameters, the obtained quantities are consistent with the experimental data. The spectrum is reproduced in good overall agreement with the experimental data of Figure 2b. Other features seen in Figure 2b, namely, the oscillations in the red part of the spectrum, might be attributed to the Fabry–Perot (FP) oscillations of the TH radiation in the buried oxide layer of the silicon-on-insulator substrate. Indeed, the estimated period of the oscillations is $3\lambda_{3\omega}^2/(2nl) = 82$ nm at $\lambda_{3\omega} = 400$ nm, where $n = 1.47$ is the refractive index of SiO_2[23] and $l = 2.0$ μm is the buried oxide thickness. The multiplier of 3 rises due to the TH wavelength being considered at the fundamental, that is, tripled, wavelength. The oscillations, however, are not considered as the source of the main three-peak feature of the spectrum in Figure 2b, because the spectral distance between the observed adjacent minima (or maxima) is less than 50 nm. The FP effect was not included into the model because of the need in additional (unknown) fitting parameters, for example, the forward-to-backward THG emission ratio, which would reduce the clarity of the physics behind the observed data. The dashed curve in Figure 4e shows eq 3 plotted with the same set of parameters, except for C set to zero, to demonstrate the explicit contributions of the ED and MD to the THG spectrum. It is peculiar to observe the maximum overall THG at the high-pump-transmission wavelength; this behavior could be utilized to apply the observed nonlinear interference effects for building efficient multilayered nanostructures with improved nonlinear response. Also, a bimodal nanostructure under study could lead to a considerable improvement of frequency nondegenerate processes.[24] Although the reported nanostructures provide relatively modest conversion efficiency of approximately 10^{-10}, which is not at the level of subdamage-threshold plasmonic nanoantennae yet,[25] the resonant silicon-based platform under study is barely restricted by linear Ohmic losses, making it a very promising candidate for high-power applications within nanophotonics.

In conclusion, we have experimentally studied the third-harmonic generation in all-dielectric oligomers composed of three silicon nanodisks. We have demonstrated that both electric and magnetic Mie-type resonances of nanodisk trimers can substantially enhance the intensity of the generated third-harmonic field. We have further observed the interplay of both electric and magnetic resonances with a strong reshaping of the third-harmonic spectra, and analyzed the dependence on the distance between the nanoparticles in the structure. We expect that, by tailoring the mutual position of the trimer Mie-type resonances, one can achieve additional flexibility in tuning nonlinear response of novel low-loss photonic nanostructures and metasurfaces.

METHODS

Sample Preparation. The samples were fabricated via electron-beam lithography on silicon-on-insulator wafers followed by reactive-ion etching. The procedure is similar to the one found in our previous works.[21] Each nanostructured square area had a footprint of 200 μm × 200 μm and contained a total of 10^4 nanodisk trimers arranged in a square lattice with a lattice constant of 2 μm. The sample dimensions as determined from SEM images are given in Table 1.

Transmittance Spectroscopy and Third-Harmonic Generation Spectroscopy. Optical properties of the silicon nanodisk trimer samples were examined using a setup for transmittance spectroscopy and THG spectroscopy. Radiation from an incandescent light source was focused at the plane of the sample at normal incidence to a 20 μm spot. The transmitted beam was collected and transferred to a grating InGaAs-based-CCD spectrometer. The spectrum measured from the sample area was normalized to the spectrum obtained for the area with no trimers. THG spectra were obtained using the same setup by focusing a train of wavelength-tunable femtosecond laser pulses to the same point of the sample to a waist of about 10 μm in diameter. The peak intensities of the chopper-modulated beam reached 8 GW/cm^2. THG signal was lock-in detected by a photomultiplier. The detailed description of the setup is given in the Supporting Information.

ASSOCIATED CONTENT

Supporting Information

A detailed description of the transmission spectroscopy measurements, THG spectroscopy measurements, evaluation of eq 3, and multipole decomposition results. The Supporting Information is available free of charge on the ACS Publications website at DOI: 10.1021/acsphotonics.5b00065.

AUTHOR INFORMATION

Corresponding Author

*E-mail: shcherbakov@nanolab.phys.msu.ru.

Notes

The authors declare no competing financial interest.

DOI: 10.1021/acsphotonics.5b00065
ACS Photonics 2015, 2, 578–582

■ ACKNOWLEDGMENTS

The authors acknowledge useful discussions with M. Kauranen, N. Panoiu, and A. Zayats, as well as the financial support from Russian Science Foundation (Grant #14-12-01144), Russian Foundation for Basic Research, and the Australian Research Council. This work was performed, in part, at the Center for Integrated Nanotechnologies, an Office of Science User Facility operated for the U.S. Department of Energy (DOE) Office of Science. Sandia National Laboratories is a multiprogram laboratory managed and operated by Sandia Corporation, a wholly owned subsidiary of Lockheed Martin Corporation, for the U.S. Department of Energy's National Nuclear Security Administration under contract DE-AC04-94AL85000.

■ REFERENCES

(1) Kauranen, M.; Zayats, A. V. Nonlinear Plasmonics. *Nat. Photonics* **2012**, *6*, 737−748.
(2) van Nieuwstadt, J. A. H.; Sandtke, M.; Harmsen, R. H.; Segerink, F. B.; Prangsma, J. C.; Enoch, S.; Kuipers, L. Strong Modification of the Nonlinear Optical Response of Metallic Subwavelength Hole Arrays. *Phys. Rev. Lett.* **2006**, *97*, 146102.
(3) Konishi, K.; Higuchi, T.; Li, J.; Larsson, J.; Ishii, S.; Kuwata-Gonokami, M. Polarization-Controlled Circular Second-Harmonic Generation from Metal Hole Arrays with Threefold Rotational Symmetry. *Phys. Rev. Lett.* **2014**, *112*, 135502.
(4) Valev, V. K.; Silhanek, A. V.; Verellen, N.; Gillijns, W.; van Dorpe, P.; Aktsipetrov, O. A.; Vandenbosch, G. A. E.; Moshchalkov, V. V.; Verbiest, T. Asymmetric Optical Second-Harmonic Generation from Chiral G-Shaped Gold Nanostructures. *Phys. Rev. Lett.* **2010**, *104*, 127401.
(5) Metzger, B.; Hentschel, M.; Schumacher, T.; Lippitz, M.; Ye, X.; Murray, C. B.; Knabe, B.; Buse, K.; Giessen, H. Doubling the Efficiency of Third Harmonic Generation by Positioning ITO Nanocrystals into the Hot-Spot of Plasmonic Gap-Antennas. *Nano Lett.* **2014**, *14*, 2867−2872.
(6) Metzger, B.; Schumacher, T.; Hentschel, M.; Lippitz, M.; Giessen, H. Third Harmonic Mechanism in Complex Plasmonic Fano Structures. *ACS Photonics* **2014**, *1*, 471−476.
(7) Chen, S.; Li, G.; Zeuner, F.; Wong, W. H.; Pun, E. Y. B.; Zentgraf, T.; Cheah, K. W.; Zhang, S. Symmetry Selective Third Harmonic Generation from Plasmonic Metacrystals. *Phys. Rev. Lett.* **2014**, *113*, 033901.
(8) Klein, M. W.; Enkrich, C.; Wegener, M.; Linden, S. Second-Harmonic Generation from Magnetic Metamaterials. *Science* **2006**, *313*, 502−504.
(9) Feith, N.; Linden, S.; Klein, M. W.; Decker, M.; Niesler, F. B. P.; Zeng, Y.; Hoyer, W.; Liu, J.; Koch, S. W.; Moloney, J. V.; Wegener, M. Second-Harmonic Generation from Complementary Split-Ring Resonators. *Opt. Lett.* **2008**, *33*, 1975−1977.
(10) Kim, E.; Wang, F.; Wu, W.; Yu, Z.; Shen, Y. R. Nonlinear Optical Spectroscopy of Photonic Metamaterials. *Phys. Rev. B* **2008**, *78*, 113102.
(11) Reinhold, J.; Shcherbakov, M. R.; Chipouline, A.; Panov, V. I.; Helgert, C.; Paul, T.; Rockstuhl, C.; Lederer, F.; Kley, E.-B.; Tünnermann, A.; Fedyanin, A. A.; Pertsch, T. Contribution of the Magnetic Resonance to the Third Harmonic Generation from a Fishnet Metamaterial. *Phys. Rev. B* **2012**, *86*, 115401.
(12) Kujala, S.; Canfield, B. K.; Kauranen, M.; Svirko, Y.; Turunen, J. Multipole Interference in the Second-Harmonic Optical Radiation from Gold Nanoparticles. *Phys. Rev. Lett.* **2007**, *98*, 167403.
(13) Shcherbakov, M. R.; Neshev, D. N.; Hopkins, B.; Shorokhov, A. S.; Staude, I.; Melik-Gaykazyan, E. V.; Decker, M.; Ezhov, A. A.; Miroshnichenko, A. E.; Brener, I.; Fedyanin, A. A.; Kivshar, Yu. S. Enhanced Third-Harmonic Generation in Silicon Nanoparticles Driven by Magnetic Response. *Nano Lett.* **2014**, *14*, 6488−6492.
(14) Evlyukhin, A. B.; Novikov, S. M.; Zywietz, U.; Eriksen, R. L.; Reinhardt, C.; Bozhevolnyi, S. I.; Chichkov, B. N. Demonstration of Magnetic Dipole Resonances of Dielectric Nanospheres in the Visible Region. *Nano Lett.* **2012**, *12*, 3749−3755.
(15) Kuznetsov, A. I.; Miroshnichenko, A. E.; Fu, Y. H.; Zhang, J.; Luk'yanchuk, B. Magnetic Light. *Sci. Rep.* **2012**, *2*, 492.
(16) Rose, A.; Huang, D.; Smith, D. R. Nonlinear Interference and Unidirectional Wave Mixing in Metamaterials. *Phys. Rev. Lett.* **2013**, *110*, 063901.
(17) Rose, A.; Powell, D. A.; Shadrivov, I. V.; Smith, D. R.; Kivshar, Yu. S. Circular Dichroism of Four-Wave Mixing in Nonlinear Metamaterials. *Phys. Rev. B* **2013**, *88*, 195148.
(18) Chong, K. E.; Hopkins, B.; Staude, I.; Miroshnichenko, A. E.; Dominguez, J.; Decker, M.; Neshev, D. N.; Brener, I.; Kivshar, Y. S. Observation of Fano Resonances in All-Dielectric Nanoparticle Oligomers. *Small* **2014**, *10*, 1985−1990.
(19) Boyd, R. W. *Nonlinear Optics*, 3rd ed.; Elsevier: New York, 2008.
(20) Miroshnichenko, A. E.; Flach, S.; Kivshar, Yu. S. The Fano Resonance in Plasmonic Nanostructures and Metamaterials. *Rev. Mod. Phys.* **2010**, *82*, 2257−2298.
(21) Staude, I.; Miroshnichenko, A. E.; Decker, M.; Fofang, N. T.; Liu, S.; Gonzales, E.; Dominguez, J.; Luk, T. S.; Neshev, D. N.; Brener, I.; Kivshar, Yu. S. Tailoring Directional Scattering through Magnetic and Electric Resonances in Subwavelength Silicon Nanodisks. *ACS Nano* **2013**, *7*, 7824−7832.
(22) Habteyes, T. G.; Staude, I.; Chong, K. E.; Dominguez, J.; Decker, M.; Miroshnichenko, A. E.; Kivshar, Yu. S.; Brener, I. Near-Field Mapping of Optical Modes on All-Dielectric Silicon Nanodisks. *ACS Photonics* **2014**, *1*, 794−798.
(23) Malitson, I. H. Interspecimen Comparison of the Refractive Index of Fused Silica. *J. Opt. Soc. Am.* **1965**, *55*, 1205−1209.
(24) Zhang, Y.; Wen, F.; Zhen, Y.-R.; Nordlander, P.; Halas, N. J. Coherent Fano Resonances in a Plasmonic Nanocluster Enhance Optical Four-Wave Mixing. *Proc. Natl. Acad. Sci. U.S.A.* **2013**, *110*, 9215−9219.
(25) Aouani, H.; Rahmani, M.; Navarro-Cía, M.; Maier, S. A. Third-Harmonic-Upconversion Enhancement from a Single Semiconductor Nanoparticle Coupled to a Plasmonic Antenna. *Nat. Nanotechnol.* **2014**, *9*, 290−294.

DOI: 10.1021/acsphotonics.5b00065
ACS Photonics 2015, 2, 578−582